

# Modeling Biological Tissues in LightTools

## Author

**Katherine Calabro**

R&D Engineer, Sr II, Synopsys

## 1. Introduction

As compared to the design of optical systems for non-biological applications, the design and simulation of systems that involve light interaction with biological tissue is considerably more difficult due to the volume scattering behavior of tissue. Not only are volume scattering simulations significantly more computationally intensive, but describing the optical properties of such tissue is also more complex.

This complexity is due to two primary factors: the challenge of obtaining optical measurements *in vivo* (performed directly in the body), and the challenge of de-convolving the separate scattering and absorption effects from measured optical signals.

This paper presents the most up to date compilation of research and data available in the literature regarding the optical properties of human tissue. The relevant optical, biological, and measurement details are presented to illustrate the necessary considerations that should be observed when modeling human tissue in LightTools. It also describes how this information has been incorporated into a new Human Tissue Utility. This utility aims to take some of the guesswork out of creating User Materials that model biological tissues.

## 2. Optical Properties Relevant to Tissue

The propagation of light through tissue is dominated by two contributing factors: absorption and scattering. The Beer-Lambert law well describes the loss of energy or power due to absorption:

$$P(\lambda) = P_0(\lambda)e^{-\mu_a(\lambda)L} \quad (1)$$

Where  $\mu_a$  is the absorption coefficient which represents the probability of absorption as a function of propagation length (units:  $\text{cm}^{-1}$ ), and  $L$  is the total path length. In the absence of scattering, this path length would be a single linear path through the material, but with scattering, it is the sum of all the paths between scattering events.

## 2.1. Absorption by Chromophores in Tissue

The absorption of light in a medium is dictated by its chemical composition, and more specifically, the chromophores present. The total absorption coefficient,  $\mu_a$ , depends on the concentration of each constituent chromophore,  $c_i$ , and its inherent wavelength-dependent molar absorptivity (a.k.a extinction coefficient),  $\epsilon_i(\lambda)$ . This relationship is quantitatively described by [1]:

$$\mu_a(\lambda) = \ln(10) \sum_{i=1}^N c_i \epsilon_i(\lambda) \quad (2)$$

where N is the total number of different chromophores in the sample. Concentration,  $c$ , is in units of moles per unit volume (or Molar concentration, M), and  $\epsilon_i(\lambda)$  is in units of  $1/(\text{length} \cdot \text{M})$ , giving  $\mu_a$  units of  $1/\text{length}$ . As a bulk property,  $\mu_a$  represents the probability of photon absorption per unit path length, or viewed alternatively,  $1/\mu_a$  is the mean free path a photon travels before being absorbed.

In tissue, absorption is dominated by oxy- and deoxy- hemoglobin in the visible range, and by water in the near infrared range (Figure 1). Less abundant sources of absorption arise from beta carotene, a component found in fat, melanin, which gives color to hair and skin, bile which is found primarily in the liver, and collagen. The total absorption of a tissue is then calculated from the linear combination of the various absorption spectra as scaled by the concentration of each chromophore. Figure 1 plots the absorption spectra or extinction coefficient of each of the constituent chromophores across the visible and near infrared wavelength ranges [1]–[5].

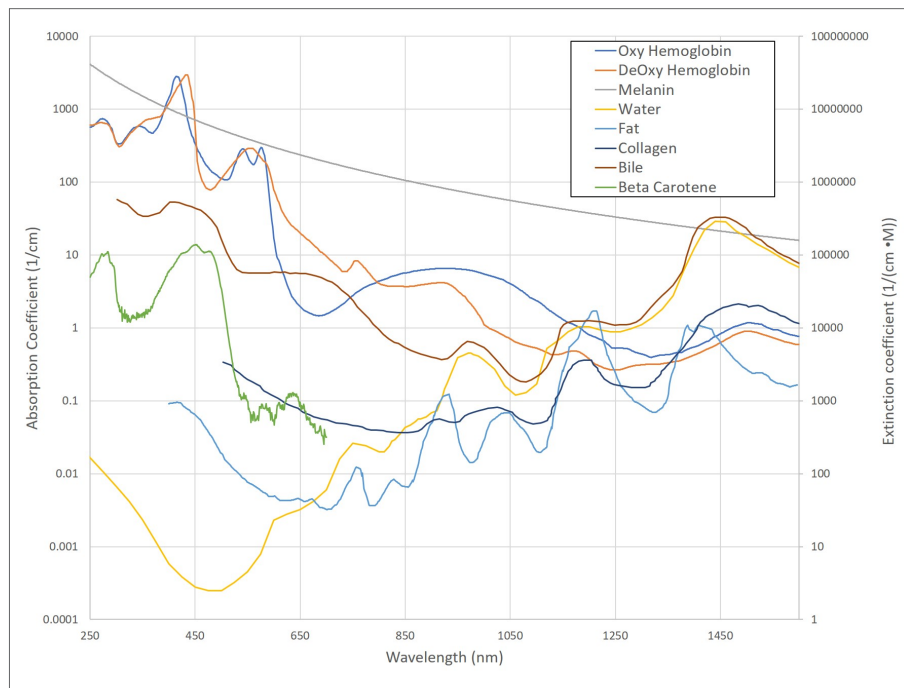


Figure 1: Absorption Coefficient spectra for Oxy and Deoxy Hemoglobin, Melanin, Water, Fat, Collagen, Bile, and the Extinction Coefficient spectra for Beta Carotene.

The distinction between an Absorption Coefficient spectrum and an Extinction Coefficient spectrum is subtle, but important. For components that have well defined molecular structures and correlated concentrations, such as beta carotene, it is traditional to use equation (2) to calculate the absorption coefficient contribution, using the exact molar concentration. But for components that don't have well-defined concentrations or molar extinction coefficients, the absorption coefficient contribution can be estimated as:

$$\mu_a(\lambda) = F_v \mu_{a,whole}(\lambda) \quad [3]$$

where  $\mu_{a,whole}$  is the absorption coefficient of a pure sample of the chromophore, and  $F$  is the volume fraction of that component within a sample. This approach actually simplifies the characterization of tissue because the volume fraction can be estimated from physiological knowledge of the tissue, and is bounded within the range [0-1]. Conversely, for components that are defined via extinction coefficient, it is necessary to know the molar concentration within a sample, which is less intuitive because the range of appropriate molar concentration values depends on the component. Ultimately, calculating absorption using an absorption coefficient spectrum and volume fraction or an extinction coefficient spectrum and molar concentration is contingent on the data available in the literature.

Taken together, the combined absorption of a given tissue sample can be calculated as:

$$\mu_a(\lambda) = B(S\mu_{a,HbO}(\lambda) + (1 - S)\mu_{a,Hb}(\lambda)) + W\mu_{a,water}(\lambda) + F\mu_{a,fat}(\lambda) + M\mu_{a,melanin}(\lambda) + L\mu_{a,bile}(\lambda) + C\mu_{a,collagen}(\lambda) + 2.3C_{\beta C}\epsilon_{\beta C}(\lambda) \quad [4]$$

where  $\mu_{a,HbO}$ ,  $\mu_{a,Hb}$ ,  $\mu_{a,water}$ ,  $\mu_{a,fat}$ ,  $\mu_{a,melanin}$ ,  $\mu_{a,bile}$ , and  $\mu_{a,collagen}$  are the absorption coefficients of oxygenated hemoglobin, deoxygenated hemoglobin, water, fat, melanin, bile, and collagen, respectively. For oxy and deoxy hemoglobin, the absorption coefficient spectra are calculated from the molar extinction coefficients of oxy- and deoxy- hemoglobin ( $\epsilon_{HbO}, \epsilon_{Hb}$ ), the average concentration of hemoglobin in the blood (150 g/L), and the molar concentration of hemoglobin (64,500 g/L) using the relationship:  $\mu_{a,Hb/HbO} = 0.0054\epsilon_{Hb/HbO}$ . [1] The coefficients  $B$ ,  $W$ ,  $F$ ,  $M$ ,  $L$ , and  $C$  are the volume fractions of blood, water, fat, melanin, bile, and collagen, respectively. The coefficient  $S$  is the oxygen saturation of the blood:  $S = [HbO_2] / ([HbO_2] + [HbO])$ , where the brackets represent concentration.

There are of course a vast number of other chromophores within the body, for example bilirubin, but the components included in equation [4] are the ones that are most dominant, and for which there is data available in the literature.

### 2.1.1. Vessel Packing Factor

When considering bulk tissue properties like  $\mu_a$ , the distribution of chromophores is assumed to be homogeneous. However, in reality, tissue is generally heterogeneous. This becomes a problem especially when considering that blood is confined within blood vessels. It has been observed that the effective absorption coefficient of a tissue with hemoglobin packed into vessels is not equivalent to the absorption coefficient of a sample in which the same amount of blood is homogeneously distributed throughout the volume. This is known as the vessel packing effect, and has been examined by a number of authors who have developed scaling relationships to account for the decrease in effective absorption coefficient as a function of average blood vessel radius,  $r$  (the effect is stronger for larger absorption coefficients and larger blood-vessel radii). The mostly commonly applied expression was developed by Svaasand et.al. [6]:

$$C_{corr}(r, \lambda) = \left\{ \frac{1 - \exp(-2\mu_{a,bl}(\lambda)r)}{2\mu_{a,bl}(\lambda)r} \right\} \quad (5)$$

where  $\mu_{a,bl}$  is the absorption coefficient of whole blood,  $\mu_{a,bl}(\lambda) = S\mu_{a,HbO}(\lambda) + (1-S)\mu_{a,Hb}(\lambda)$ . The effective absorption coefficient is then:

$$\mu_{a,Hemoglobin}(\lambda) = BC_{corr}(r, \lambda)\mu_{a,bl}(\lambda) \quad (6)$$

Since the correction factor is a function of both wavelength and radius, the scaling amount will be different at each wavelength resulting in a change in the spectral shape of the hemoglobin absorption curves. As an example, in the Soret absorption band (around 425nm) the absorption coefficient of whole blood is just under  $3000\text{cm}^{-1}$ . If a capillary radius of  $5\mu\text{m}$  is assumed, the correction factor is equal to 0.32, or in other words, the effective  $\mu_a$  under these conditions is one third of what would be expected if the blood was homogeneously distributed. In contrast, at a wavelength of 650nm, the absorption coefficient of whole blood is approximately  $10\text{cm}^{-1}$ , which results in a correction factor of 0.99.

With this additional factor, equation [4] can be modified as:

$$\begin{aligned} \mu_a(\lambda) = & BC_{corr}(S\mu_{a,HbO}(\lambda) + (1 - S)\mu_{a,Hb}(\lambda)) + W\mu_{a,water}(\lambda) + F\mu_{a,fat}(\lambda) \\ & + M\mu_{a,melanin}(\lambda) + L\mu_{a,bile}(\lambda) + C\mu_{a,collagen}(\lambda) + 2.3c_{\beta c}\epsilon_{\beta c}(\lambda) \end{aligned} \quad (7)$$

## 2.2. Scattering in Tissue

Scattering in tissue is considered in equation [1] via the total path length,  $L^*$ . Quantifying this value analytically is not well defined given the stochastic nature of scattering. This is particularly true in diffuse reflectance geometries which represent most *in vivo* scenarios for which light is both illuminated on and collected from the same tissue surface. Scattering can be further decomposed into two factors: mean free path (MFP) and phase function. The MFP describes the average distance a photon propagates before encountering a scattering event. In the bio-optics literature, it is most commonly presented as the scattering coefficient,  $\mu_s$ , which analogous to the absorption coefficient, represents the probability of scattering as a function of propagation length (units:  $\text{cm}^{-1}$ ). It is related to MFP:

$$\mu_s = 1/MFP \quad (8)$$

The phase function,  $p(\theta)$ , of a volume scattering material defines the probabilistic distribution of angles that dictates the change in direction of a photon at scattering events. Such distributions can be mathematically defined either analytically from fundamental principles via Mie Theory, or generalized via more simplistic parameterized functions. If one were to expand the phase function as a series of Legendre Polynomials,  $P_n(\cos\theta)$ :

$$p(\cos\theta) = \frac{1}{4\pi} \sum_n (2n + 1)g_n P_n(\cos\theta) \quad (9)$$

the  $n$ th-order Legendre moments can then be used to define the moments of the phase function.

$$g_n = 2\pi \int_0^\pi P_n(\cos\theta) p(\cos\theta) \sin\theta d\theta \quad (10)$$

The first phase function moment,  $g_1$ , is equivalent to the commonly referred to anisotropy factor,  $g$ . A phase function with  $g=1$  represents complete forward scattering, and  $g=0$  represents a balance of forward and backward scattering (i.e. isotropic scattering).

### 2.2.1. Similarity Conditions

The definition of phase function moments becomes useful for describing similarity parameters. The most useful similarity parameter used in bio-optics is that of the 'reduced scattering coefficient,' which is defined as:

$$\mu'_s = (1 - g_1)\mu_s \quad (11)$$

Since the phase function moments are unitless, the reduced scattering coefficient also has units of inverse length. Its inverse, the reduced mean free path,

$$MFP' = 1/\mu'_s = \frac{MFP}{(1 - g_1)} \quad (12)$$

can be thought of conceptually as the average distance a photon travels before it undergoes a significant change in direction. Or in other words, it is the average distance between effectively isotropic scattering events[7]. Under certain diffuse conditions, this reduced scattering similarity condition indicates that measured illuminance will be equivalent for equal values of  $\mu'_s$ , regardless of the values of  $g_1$  and  $\mu_s$ . For example, under this similarity condition, measured illuminance will be the same for two tissue samples: one with  $\mu_s=10 \text{ cm}^{-1}$  and  $g_1=0$ , and the other with  $\mu_s=100 \text{ cm}^{-1}$  and  $g_1=0.9$ , since both samples have  $\mu'_s=10 \text{ cm}^{-1}$ .

## 2.2.2. Henyey-Greenstein

The most popular analytical phase function representation used for simulation of tissue is the Henyey-Greenstein phase function due to its simplicity. Originally developed to describe the scattering from interstellar dust particles[8], it is a simple one parameter function whose single variable,  $g$ , is equal to the anisotropy factor.

$$p_{HG}(\cos \theta) = \frac{1}{4\pi} \frac{1 - g^2}{(1 + g^2 - 2g \cos \theta)^{3/2}} \quad (13)$$

The simplicity of this formulation is both advantageous (only a single parameter is necessary), and disadvantageous (it has been shown to underestimate high angle backscattering events). Unfortunately, phase function is the single most difficult piece of data to measure accurately in tissue. Measured data reporting the  $g$  value in tissue is extremely limited, with phase function measurements of higher order moments ( $g_2$ , etc.) being almost non-existent. This is why focusing our tissue modeling on the combined effects of  $\mu_s$  and  $g$ , in the form of the reduced scattering coefficient ( $\mu'_s$ ) is so advantageous; uncertainty in measurements for both  $\mu_s$  and  $g$  are reduced by focusing on their combined effect in the form of  $\mu'_s$ .

This is not to say that the choice of phase function is irrelevant. In fact, much work has been done highlighting the importance of phase function, and models have been built to incorporate the dependence[9], [10]. However, the measurement and availability of *in vivo* data has not yet caught up to the theoretical understanding.

## 2.2.3. Wavelength Dependent Assumptions

Unlike absorption, there is no well-defined analytical relationship that can be used to define the spectral dependence of volume scattering. However, based on experimental observations and simplifying analysis of Mie Scattering Theory, there is a consensus that the reduced scattering coefficient can be modeled using a power law relationship [1]:

$$\mu'_s = a \left( \frac{\lambda}{\lambda_0} \right)^{-b} \quad (14)$$

The incorporation of  $\lambda_0$  allows for the variable 'b' to be dimensionless, so that 'a' represents the reduced scattering coefficient at  $\lambda_0$ . When the distribution of particles is skewed towards small particle sizes, 'b' approaches the value 4 (for Rayleigh Scattering), and when the distribution is skewed towards larger particle sizes, 'b' approaches 0.37 [11], [12]. Thus, the value of 'b' can provide a rough indication about the mean size of the particles in the sample, but only if the distribution is not broad. For size distributions where both small and large particle sizes are represented, it has been proposed to model the wavelength dependence of the reduced scattering coefficient as a combination of the two limiting cases as [13]–[15]:

$$\mu'_s = a \left( f_{Ray} \left( \frac{\lambda}{\lambda_0} \right)^{-4} + (1 - f_{Ray}) \left( \frac{\lambda}{\lambda_0} \right)^{-b} \right) \quad (15)$$

Where  $f_{Ray}$  is the fraction of Rayleigh scattering. The choice of form is primarily dictated by the availability of measured data in the literature.

## 2.3. Refractive Index

In non-scattering materials, the refractive index spectrum is critically important. However, with the dominance of scattering in tissue, the impact of refractive index is more of a second or third order effect, primarily influencing specular surface reflectance. As such, there hasn't been significant effort to measure the refractive index of tissue *in vivo*. Rather, assumptions have been made based on knowledge of the composition of tissue. Considering tissue to be a mix of water and 'dry' components, the refractive index of the composite tissue can be approximated as [1]:

$$n = n_{dry} - (n_{dry} - n_{water})W \quad (16)$$

where  $n_{dry}$  is the refractive index of the dry components (connective tissue, fat, etc.),  $n_{water}$  is the refractive index of water, and  $W$  is the volume fraction of water. Using 1.514 as the value of  $n_{dry}$  and 1.33 as the value of  $n_{water}$ , the refractive index reduces to a single variable relationship based on the water content of the tissue. The imaginary component of the refractive index is not considered since absorption is instead modeled using the absorption coefficient.

## 3. Estimating the Optical Property Values of Tissue

Great progress has been made recently in better understanding the critical optical properties of tissue and how they influence optical measurements under a range of geometries. However, even with this knowledge, accurately simulating tissue remains a challenge due to the lack of reliable experimental data. Measuring the properties of tissue directly is made difficult by the heterogeneous nature of tissue, and the challenge of deconvolving the effects of scattering and absorption. Further, especially if *in vivo* data is desired, it is not possible to perform measurements in a controlled environment using tools like an integrating sphere, as is possible for non-biological samples. Because there is no gold standard method for measuring tissue optical properties, it is difficult to assess the accuracy of the data available in the literature.

### 3.1. Diffuse Reflectance Spectroscopy

Nonetheless, efforts continue to be made to collect data from *in vivo* tissue samples. The primary approach used is Diffuse Reflectance Spectroscopy (DRS). In its most common form, DSR involves the illumination of light from one optical fiber into a tissue sample; a fraction of that illuminated light will be collected by one or more detection fibers, as illustrated in Figure 2a. The fractional collected signal is termed 'reflectance.' The wavelengths typically used span from the near-UV through the near infrared (NIR), a range over which measurements are dominated by scattering and absorption interactions. An example reflectance spectrum is illustrated in Figure 2b. In general, an increase in scattering results in an increase in measured reflectance, and an increase in absorption leads to a decrease in reflectance. As can be seen from the spectrum, the overall spectral shape has a power law dependence, as described by the  $\mu_s$ ' relationship in equation [14]; this reflectance is attenuated around 420 nm and 550 nm by strong absorption from hemoglobin.

The relationships between scattering and absorption vs. reflectance can be described via analytical/empirical equations or via numerical lookup table (the data primarily coming from Monte Carlo raytracing simulations)[16]–[18]. Using these relationships, a measured reflectance spectrum can then be fit via least squares curve fitting (i.e. optimization) to extract the coefficients that describe the scattering and absorption spectra from equations (7) and (14) or (15). These DSR measurements are a relatively simple, cost effective way to estimate optical properties of small volumes of tissue; more complicated is gaining access to the tissue of interest within the body with the fiber optic probe, handling the red tape associated with medical research on human subjects, and assessing the accuracy of the extracted results without alternative validation techniques.

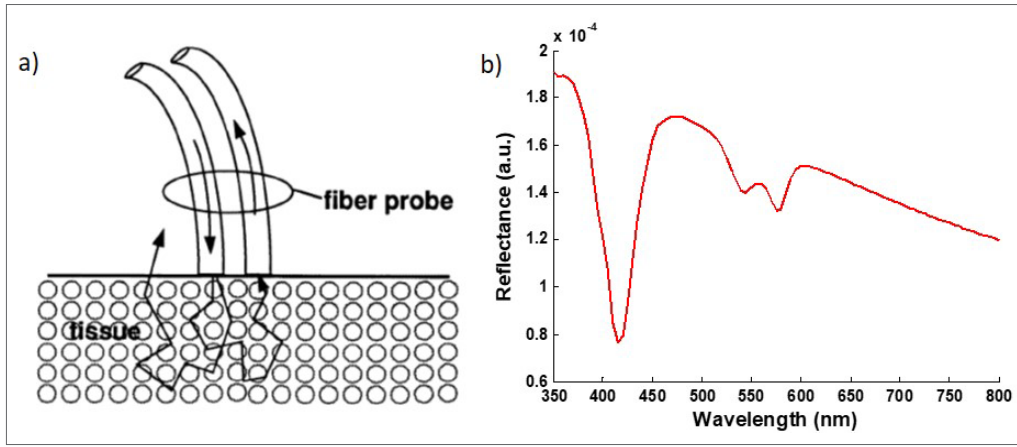


Figure 2: a) Measurement Geometry for Diffuse Reflectance Spectroscopy  
 b) example reflectance spectrum. Reproduced from [17].

### 3.2. Human Tissue Data in the Literature

To date, the best source of tissue measurements is a review article published by Steven Jacques [1]. It is the most comprehensive set of tissue optical property data currently available in the literature, and reports not only on data at single wavelengths, but also provides estimates for wavelength dependencies. It presents the data using the same wavelength dependent relationships outlined in Section 2 (equations (7), (14), (15), (16)), such that the tissues can be fully characterized with the variable coefficients  $B$ ,  $S$ ,  $r$ ,  $W$ ,  $F$ ,  $M$ ,  $L$ ,  $C$ ,  $c_{\beta c}$ ,  $a$ ,  $b$ , and  $f_{\text{Ray}}$  (Blood volume fraction, blood oxygen saturation, average blood vessel radius, water volume fraction, fat volume fraction, melanin volume fraction, bile volume fraction, collagen volume fraction, molar concentration of Beta Carotene, power law variable  $a$ , power law variable  $b$ , and the fraction of Rayleigh scattering). Since its publication in 2013, a handful of other studies have been published providing data for more tissue types. Tables 1 and 2 provide summaries of the coefficients that describe absorption and scattering in tissue, respectively[1], [2], [25]–[28], [3], [5], [19]–[24].

Tissue Type	$a$ (1/cm)	$b$	$f_{\text{Ray}}$	$\lambda_0$	$g$
Whole Blood	825.00	1.23	0.00	700	0.98
Bone	8.37	0.64	0.00	600	0.93
Generic Skin Very Fair (Type I-II)	48.00	0.70	0.41	500	0.92
Generic Skin Medium (Type III-IV)	48.00	0.70	0.41	500	0.92
Generic Skin Dark (Type V-VI)	48.00	0.70	0.41	500	0.92
Skin Dermis	43.60	0.56	0.41	500	0.92
Skin Epidermis	66.70	0.69	0.29	500	0.92
Brain (general)	27.40	1.09	0.32	500	0.90
Muscle	4.60	0.60	0.13	800	0.97
Fatty tissue (including subcutaneous tissue)	19.30	0.45	0.17	500	0.95
Esophagus/Stomach	19.10	1.09	0.02	500	0.95
Lungs	44.00	0.98	0.00	800	0.95
Liver	17.00	1.20	0.56	800	0.90
General Soft Tissue	19.10	1.09	0.02	500	0.95
Breast (general)	18.70	0.69	0.19	500	0.96
Fibrous Breast	17.60	1.16	0.00	600	0.96
Adipose Breast	37.33	0.61	0.00	600	0.96

Table 1: Summary of Scattering Variables of various Tissue Types as reported in the literature.

Tissue Type	B	S	r (cm)	W	F	L	M	C	$c_{\beta c}$ ( $\mu\text{M}$ )
Whole Blood	1	0.98	0	0.21	0	0	0		0
Bone	0.0124	0.72	0	0.31	0.80	0	0	0.041	0
Generic Skin Very Fair (Type I-II)	0.0025	0.94	0.0010	0.21	0.25	0	0.008		100
Generic Skin Medium (Type III-IV)	0.0025	0.94	0.0010	0.21	0.26	0	0.010		100
Generic Skin Dark (Type V-VI)	0.0025	0.94	0.0010	0.20	0.23	0	0.015		100
Skin Dermis	0.0020	0.39	0.0010	0.65	0.25	0	0		70
Skin Epidermis	0	0.00	0	0.15		0	0.025		210
Brain (general)	0.0200	0.65	0.0010	0.80	0.12	0	0		
Muscle	0.0080	0.21	0.0019	0.82	0.18	0	0		
Fatty tissue	0.0080	0.21	0.0015	0.35	0.65	0	0		
Esophagus/Stomach	0.0360	0.90	0.0030	0.70	0.05	0	0		1.6
Lungs	0.1700	0.67	0.0010	0.58		0	0		
Liver	0.0320	0.08	0.0053	0.76	0.19	0.055	0		
General Soft Tissue (bowel, heart, kidney)	0.0100	0.90	0.0010	0.50	0.20	0	0		
Breast (general)	0.0098	0.67	0.0010	0.16	0.62	0	0		8
Fibrous Breast	0.0104	0.80	0.0010	0.62	0.19	0	0	0.055	
Adipose Breast	0.0049	0.75	0.0015	0.10	0.74	0	0	0.019	

Table 2: Summary of Absorption Variables of various Tissue Types as reported in the literature.

### 3.3. Interpretation of Literature Data

- In Table 1, if the value of  $f_{\text{Ray}}$  is 0, that indicates that the scattering coefficient relationship is described using equation (14), and otherwise, equation (15) should be used.
- Values for the anisotropy factor,  $g$ , are the most difficult to measure *in vivo*, and as such are not well reported in the literature. As mentioned in section 2, specifying scattering using the reduced scattering coefficient helps to minimize the effects of uncertainty in  $g$ , but still, this is a variable that remains difficult to accurately model. Values of  $g$  range from approximately 0.85 to 0.99 for almost all tissues, and so in cases where data for a particular tissue type is not specifically documented,  $g$  is estimated based on data from similar tissue types.
- Similarly, for the average blood vessel radius, not every study incorporates the correction factor, and so blood vessel radius is only available for a handful of tissue types. For consistency in our data set, when data was not available for a tissue type, values were estimated based on data from similar tissue types.
- The values in the literature for absorption do not provide data consistently for the same set of chromophores. This is because studies were focused on different wavelength ranges; study authors made assumptions about which chromophores were the most dominant in a particular wavelength range, including only those that were deemed significant. In certain cases, it is safe to make assumptions about a particular chromophore having zero contribution (i.e. bile is primarily a liver chromophore, and melanin is primarily a skin chromophore). However, particularly for collagen and beta carotene, a lack of data does not necessarily indicate an absence of that chromophore. In Table 2 above, for entries with a zero value, it can safely be assumed that chromophore has minimal influence on absorption. For the data entries that are blank, there simply isn't enough data to make an estimate.
- Fat is not technically a chromophore in the same way that hemoglobin, or beta carotene are chromophores; it represents a category of tissue physiologically, not chemically. However, multiple studies have used the average absorption spectra of fat (as measured from purified fat samples), treating it as a single chromophore. The advantage is that it is easier to estimate the volume fraction of fat in a tissue than concentrations of the multiple chromophores that contribute to its absorption. One of these chromophores is beta carotene. The absorption spectrum for beta carotene is only available for lower wavelengths (approximately  $< 500\text{nm}$ ), while the spectrum for fat is available for wavelengths above  $500\text{nm}$  (see Figure 1). Thus, studies that analyzed data from the visible wavelength range will report beta carotene concentrations, whereas studies that analyze

data from the NIR report fat volume fractions. There is no trivial way to convert between the two metrics because beta carotene concentration is not known specifically for fat, and because beta carotene is found in tissues other than fatty tissue. Fortunately, in our data set, there is not significant overlap in the two spectra, and so it is reasonable to include contributions for both beta carotene concentration and fat volume fraction without concern of ‘double counting.’

Figure 3a) presents the calculated reduced scattering coefficient spectra using equations (14) and (15) and the coefficients in Table 1. Figure 3b-d) present the calculated absorption spectra using equation (7) and the coefficients in Table 2. To improve visibility, the absorption spectra are shown using multiple plots, broken up roughly by similar tissue types.

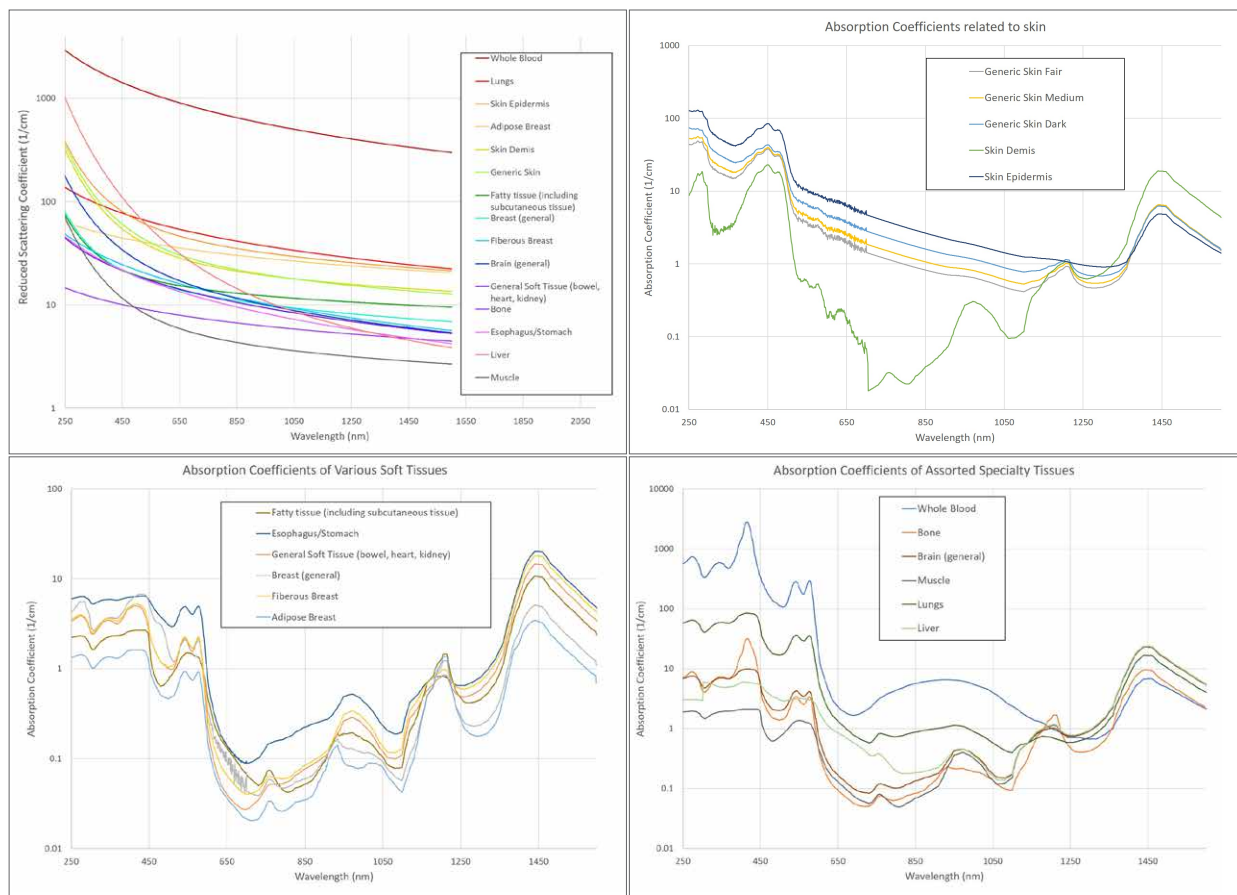


Figure 3: Calculated reduced scattering (a) and absorption (b-d) spectra as calculated with equations (7), (14), and (15), using the literature coefficient data in Tables 1 and 2.

The plots in Figure 3 demonstrate that the scattering and absorption spectra of tissue have more commonalities than differences. For scattering, the primary difference is simply that of amplitude. Similarly, for absorption, amplitude is the primary differentiator, with the relative contributions from blood, water, and melanin providing most of the shape differences.

To better understand how the contributions of various chromophores influence the total absorption spectrum, Figure 4 presents, as an example, the absorption spectra of all the component chromophores along with the total absorption spectrum of Fibrous Breast Tissue. Notice that the dominant chromophore in the visible range is Hemoglobin, while water is the dominant chromophore in the IR. The remaining chromophores have secondary effects on the spectrum.

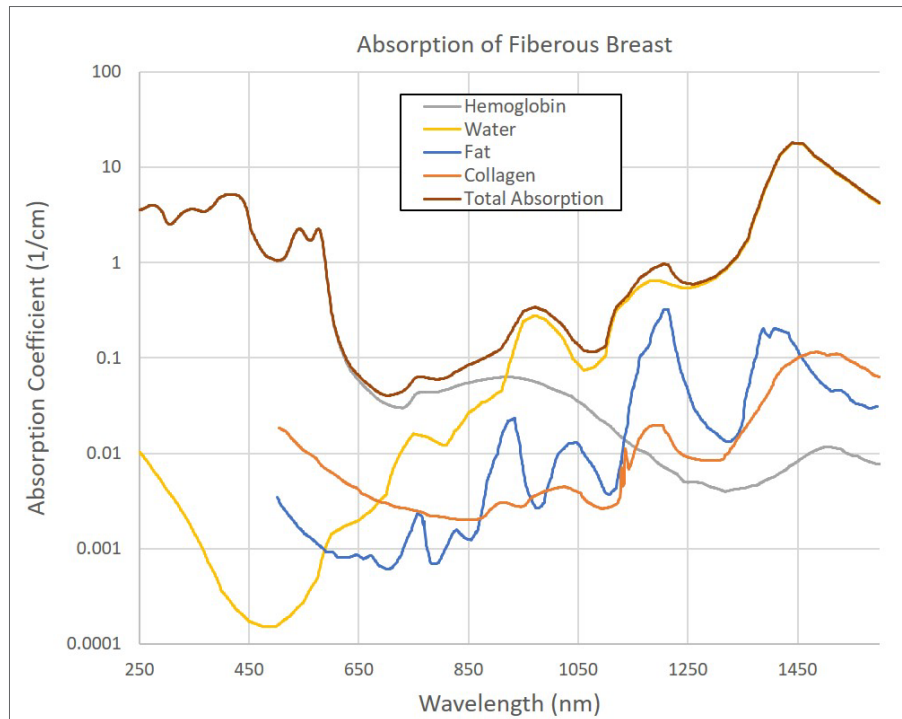


Figure 4: The component and total absorption spectra for Fibrous Breast Tissue

### 3.4. Data Variability

While the data compiled in Tables 1 and 2 represent the best data currently available in the literature, variability within the data sets is significant due to differences in measurement techniques, and the inherent difficulty in measuring tissue *in vivo*. For example, in Jacques[1], where data is compiled from multiple studies, the standard deviations of the data coefficients (a, b, etc.) are about 40% of the reported value. Part of this inconsistency can be attributed to experimental errors, but another significant source of variation is biological variability. Most obviously, differences exist between different subjects depending on age, body composition, health, etc. But even for a single patient, the optical properties can have considerable differences from point to point within the same organ. The consequence of this inherent uncertainty is that when performing simulations, one must consider a range of likely optical properties and design systems with such variations in mind.

## 4. Human Tissue Utility in LightTools

Given all the complexities of modeling human tissues, LightTools provides a utility to help users build User Materials that better represent biological materials. The Human Tissue Utility (HTU) uses the theory and data available in the literature that has been presented here. Of particular note, LightTools does not currently allow for User Materials to contain multiple absorbing components; it is restricted to a single absorption spectrum. Because of the multiple chromophore nature of tissue, one of the most powerful aspects of the HTU is the ability to combine multiple absorption spectra, scaling each spectra separately based on concentration.

The HTU is designed to model tissue using the following assumptions:

- Refractive Index: Calculates the constant refractive index based on the water volume fraction (Equation (16)).
- Absorption: Calculates the combined absorption spectra using Equation (7) with inputs for blood volume fraction, blood oxygen saturation, average blood vessel radius, water volume fraction, fat volume fraction, melanin volume fraction, bile volume fraction, collagen volume fraction, and molar concentration of Beta Carotene. It is also possible to add additional user-defined chromophores. The built-in chromophores are the most common ones found in tissue, but certainly not the only ones. For example, bilirubin is a secondary chromophore that can be found in neonatal skin due to the condition of Jaundice. Additional chromophores can be added either as an absorption coefficient and volume percent pair, or as an extinction coefficient and Molar concentration pair.

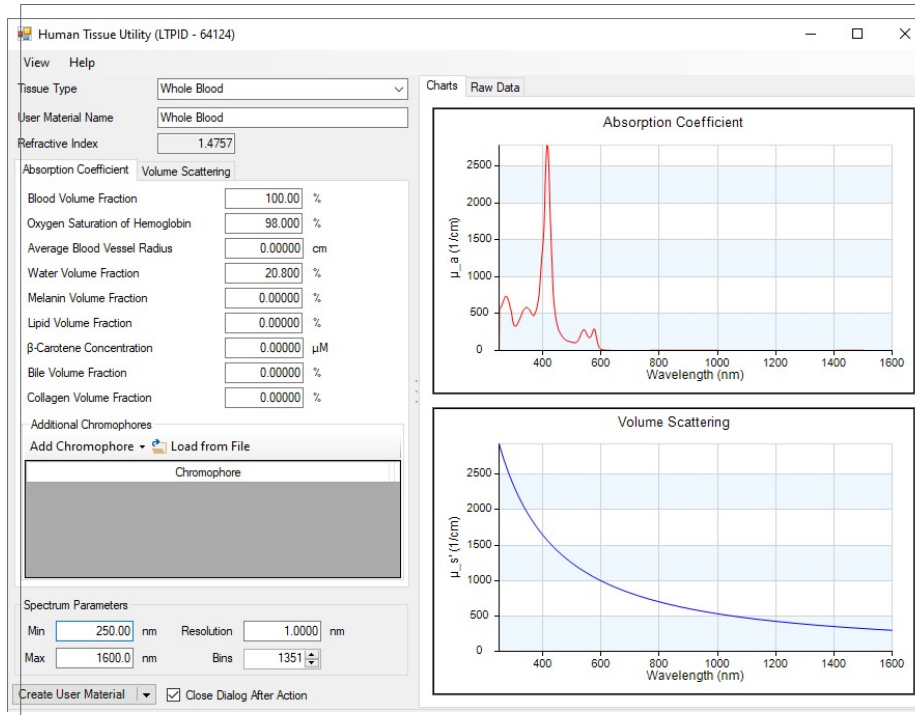


Figure 5: Screenshot of the Human Tissue Utility showing the Absorption Coefficient input variables.

- Scattering: Calculates the Reduced Scattering Coefficient spectrum from Equations (14) (Simple Power Law) and (15) (Power Law Plus Rayleigh). The choice of Simple Power Law or Power Law Plus Rayleigh is user defined and is dependent almost entirely on what data is available in the literature. The scattering phase function is defined using the Henyey-Greenstein equation and the anisotropy factor variable,  $g$ . Because of lack of experimental data, the HTU assumes the anisotropy factor is constant over the wavelength range.

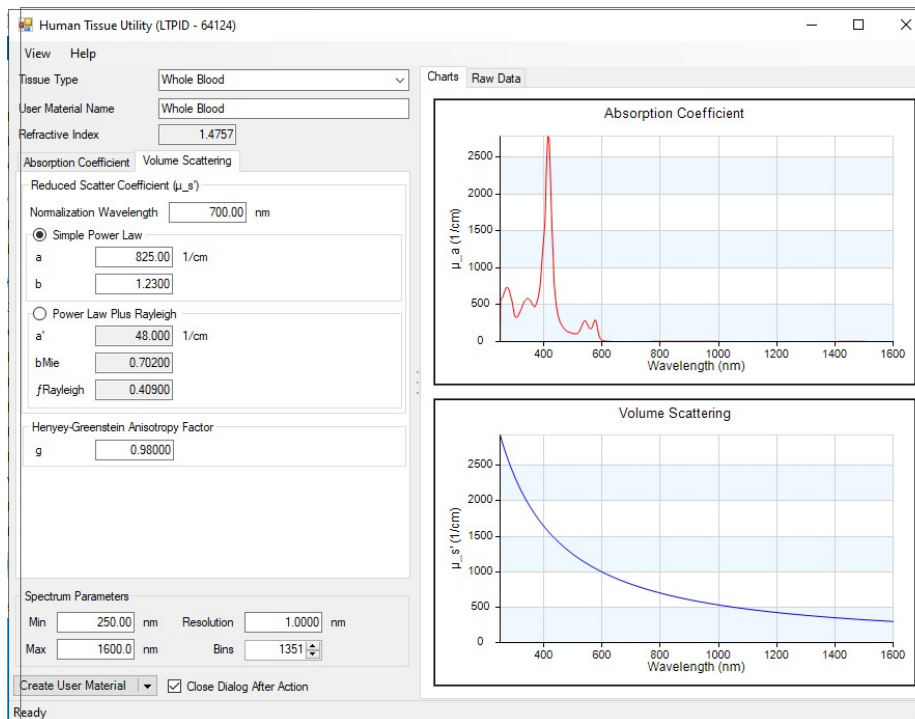


Figure 6: Screenshot of the Human Tissue Utility showing the Scattering input variables.

- The wavelength range and resolution can be customized, but due to limitation of chromophore data, the maximum range is from 250nm to 1600nm. Refer to Figure 1 for the available spectral ranges for the individual chromophores.

The output of the HTU is a custom User Material defined with a constant refractive index, absorption defined as an Absorption Coefficient spectrum, and a Henyey-Greenstein particle that defines the scattering distance with a Reduced Scattering Coefficient spectrum.

As emphasized earlier, variability of the data is high, and the values prepopulated in the utility should be viewed only as a starting point. To that end, the HTU is also capable of creating optimization and tolerance variables from the coefficient values in the utility. It is strongly encouraged that any design involving human tissue should also incorporate a tolerancing analysis to ensure proper performance over the wide data range.

For some tissue types prepopulated in the utility, there are average or 'general' data values as well as more specific component data values. For example, the data for 'General Skin' is the bulk average of all skin layers, whereas the data for Epidermis and Dermis represent the properties of those individual layers. The choice of whether to model the skin as a single homogeneous material versus a layered structure depends on many factors such as the wavelength range and the distance between the light source and detector. These factors primarily affect the penetration depth of the light that is collected. Wavelengths corresponding to lower absorption tend to penetrate more deeply; the range from 650nm to 1350nm is commonly known as the 'optical window' or 'therapeutic window' because of the greater penetration depth of light and lower attenuation, allowing for greater ability to collect useful optical signal.

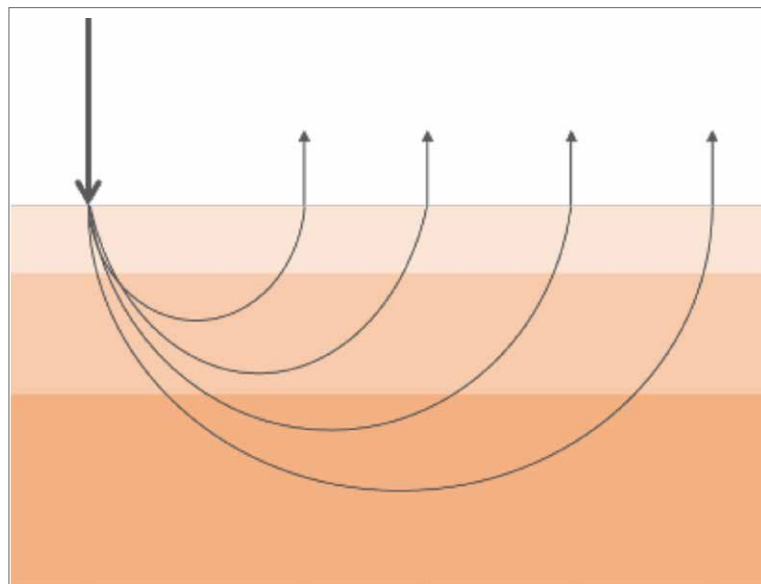


Figure 7: Schematic demonstrating how distance between the entering and exiting location of light in a layered tissue structure affects the penetration depth and relative contribution of signal from each layer.

Similarly, the penetration depth is dependent on the distance between the entering and exiting locations of the light. Light collected closer to the source will have a shallower penetration depth, and light collected further from the source will penetrate more deeply. A shallower penetration depth will be more influenced by the top layers, and a deeper penetration depth will be influenced by all layers more evenly, as demonstrated in Figure 7. Work is ongoing to identify more specific guidelines as to when the homogeneous 'general' tissue assumption is sufficient versus when the heterogenous layered tissue is necessary for accurate simulations.

## 5. Conclusion

The field of biomedical optics is still relatively new, having gained momentum in only the last 25 years. And as the challenges of collecting and analyzing data from human tissue is plagued by many complications, knowledge about how to most accurately model biological material is limited. The methods and data presented here represents the current best practices in the field, albeit incomplete.

Despite the lack of experimental data, the framework that has been leveraged in the Human Tissue Utility still represents a significant step forward. And because the data is defined not as static sets of spectral measurements, but instead using wavelength dependent relationships and variables that are physiologically representative, updating or 'tweaking' the data sets is relatively straightforward. Further, for tissue types not pre-populated in the utility, users can make educated assumptions based on the composition of the tissue.

## 6. References

- [1] S. L. Jacques, "Optical properties of biological tissues: a review.," *Phys. Med. Biol.*, vol. 58, no. 11, 2013.
- [2] R. Nachabé et al., "Effect of bile absorption coefficients on the estimation of liver tissue optical properties and related implications in discriminating healthy and tumorous samples," *Biomed. Opt. Express*, vol. 2, no. 3, p. 600, Mar. 2011.
- [3] R. Nachabé, B. H. W. Hendriks, M. van der Voort, A. E. Desjardins, and H. J. C. M. Sterenborg, "Estimation of biological chromophores using diffuse optical spectroscopy: benefit of extending the UV-VIS wavelength range to include 1000 to 1600 nm," *Biomed. Opt. Express*, vol. 1, no. 5, p. 1432, Dec. 2010.
- [4] S. Prah and S. Jacques, "Biological Spectra of various Chromophores," Oregon Medical Laser Center, 2018. [Online]. Available: <https://omlc.org/spectra/index.html>.
- [5] S. K. V. Sekar et al., "Diffuse optical characterization of collagen absorption from 500 to 1700 nm," *J. Biomed. Opt.*, vol. 22, no. 1, p. 015006, Jan. 2017.
- [6] L. O. Svaasand et al., "Therapeutic Response During Pulsed Laser Treatment of Port-wine Stains: Dependence on Vessel Diameter and Depth in Dermis," *Laser Med. Sci.*, vol. 10, pp. 235–243, 1995.
- [7] I. J. Bigio and S. Fantini, *Quantitative Biomedical Optics*. Cornwall: Cambridge University Press, 2016.
- [8] L. G. Henyey and J. L. Greenstein, "Diffuse Radiation in the Galaxy," *Astrophys. J.*, vol. 93, pp. 70–83, 1941.
- [9] K. Calabro and I. Bigio, "Influence of the phase function in generalized diffuse reflectance models: review of current formalisms and novel observations," *J. ...*, vol. 19, no. 7, p. 075005, 2014.
- [10] K. W. Calabro and W. Cassarly, "Modeling scattering in turbid media using the Gegenbauer phase function," in *Progress in Biomedical Optics and Imaging - Proceedings of SPIE*, 2015, vol. 9333.
- [11] J. R. Mourant, J. P. Freyer, A. H. Hielscher, A. A. Eick, D. Shen, and T. M. Johnson, "Mechanisms of light scattering from biological cells relevant to noninvasive optical-tissue diagnostics.," *Appl. Opt.*, vol. 37, no. 16, pp. 3586–93, Jun. 1998.
- [12] J. R. Mourant, T. Fuselier, J. Boyer, T. M. Johnson, and I. J. Bigio, "Predictions and measurements of scattering and absorption over broad wavelength ranges in tissue phantoms," *Appl. Opt.*, vol. 36, no. 4, pp. 949–957, 1997.
- [13] A. N. Bashkatov, E. A. Genina, V. I. Kochubey, and V. V Tuchin, "Optical properties of human skin, subcutaneous and mucous tissues in the wavelength range from 400 to 2000 nm," *J. Phys. D. Appl. Phys.*, vol. 38, pp. 2543–2555, 2005.
- [14] C. Lau et al., "Re-evaluation of model-based light-scattering spectroscopy for tissue spectroscopy," *J. Biomed. Opt.*, vol. 14, no. 2, p. 024031, 2009.
- [15] I. S. Saidi, S. L. Jacques, and F. K. Tittel, "Mie and Rayleigh modeling of visible-light scattering in neonatal skin," *Appl. Opt.*, vol. 34, no. 31, pp. 7410–7418, 1995.
- [16] R. Reif, O. A' Amar, and I. J. Bigio, "Analytical model of light reflectance for extraction of the optical properties in small volumes of turbid media.," *Appl. Opt.*, vol. 46, no. 29, pp. 7317–28, Oct. 2007.

- [17] K. W. Calabro, "Improved Mathematical and Computational Tools for Modeling Photon Propagation in Tissue," Boston University, 2013.
- [18] B. S. Nichols, J. W. Tunnell, and N. Rajaram, "Performance of a lookup table-based approach for measuring tissue optical properties with diffuse optical spectroscopy," *J. Biomed. Opt.*, vol. 17, no. 5, p. 057001, 2012.
- [19] P. Taroni, A. Bassi, D. Comelli, A. Farina, R. Cubeddu, and A. Pifferi, "Diffuse optical spectroscopy of breast tissue extended to 1100 nm," *J. Biomed. Opt.*, vol. 14, no. 5, p. 054030, 2009.
- [20] L. L. de Boer et al., "Using DRS during breast conserving surgery: identifying robust optical parameters and influence of inter-patient variation," *Biomed. Opt. Express*, vol. 7, no. 12, p. 5188, Dec. 2016.
- [21] J. W. Spliethoff et al., "Real-time in vivo tissue characterization with diffuse reflectance spectroscopy during transthoracic lung biopsy: A clinical feasibility study," *Clin. Cancer Res.*, vol. 22, no. 2, pp. 357–365, Jan. 2016.
- [22] A. Amelink, J. Haringsma, and H. J. C. M. Sterenberg, "Noninvasive measurement of oxygen saturation of the microvascular blood in Barrett's dysplasia by use of optical spectroscopy," *Gastrointest. Endosc.*, vol. 70, no. 1, pp. 1–6, Jul. 2009.
- [23] A. Amelink, H. J. C. M. Sterenberg, J. L. N. Roodenburg, and M. J. H. Witjes, "Non-invasive measurement of the microvascular properties of non-dysplastic and dysplastic oral leukoplakias by use of optical spectroscopy," *Oral Oncol.*, vol. 47, no. 12, pp. 1165–1170, Dec. 2011.
- [24] A. Sudakou et al., "Depth-resolved assessment of changes in concentration of chromophores using time-resolved near-infrared spectroscopy: estimation of cytochrome-c-oxidase uncertainty by Monte Carlo simulations," *Biomed. Opt. Express*, vol. 10, no. 9, p. 4621, Sep. 2019.
- [25] J. A. Iglesias-Guitian, C. Aliaga, A. Jarabo, and D. Gutierrez, "A Biophysically-Based Model of the Optical Properties of Skin Aging," 2015.
- [26] S.-H. Tseng, P. Bargo, A. Durkin, and N. Kollias, "Chromophore concentrations, absorption and scattering properties of human skin in-vivo," *Opt. Express*, vol. 17, no. 17, p. 14599, Aug. 2009.
- [27] S. Konugolu Venkata Sekar et al., "In Vivo, non-invasive characterization of human bone by hybrid broadband (600-1200 nm) diffuse optical and correlation spectroscopies," *PLoS One*, vol. 11, no. 12, Dec. 2016.
- [28] N. Bosschaart, G. J. Edelman, M. C. G. Aalders, T. G. Van Leeuwen, and D. J. Faber, "A literature review and novel theoretical approach on the optical properties of whole blood," *Lasers Med. Sci.*, vol. 29, no. 2, pp. 453–479, 2014.